山形大学紀要（工学）第32巻　平成22年２月
Bull. Yamagata Univ. (Eng.) Vol.32 Feb. 2010

Solution Structure of Apocalmodulin bound to a Binding Domain Peptide from the IQ motifs of Myosin V

Yoshinobu Izumi, Hiroki Ebisawa, Yuji Jinbo

Graduate Program of Human Sensing and Functional Sensor Engineering,
Graduate School of Science and Engineering, Yamagata University,
4-3-16 Jo-Nan, Yonezawa, Yamagata, 992-8510, Japan

（平成21年10月８日受理）

Abstract

The solution structures of complexes between apocalmodulin (apoCaM) and a binding domain of the IQ motifs of myosin V have been determined by small-angle X-ray scattering (SAXS) with use of synchrotron radiation as an intense and stable X-ray source. We used three synthetic peptides of residues 772-786 (IQ1), 795-810 (IQ2), and 772-810 (IQ(1+2)) of the myosin V to compare the solution structures with the corresponding crystal structure (PDB: 2ix7). The radius of gyration of apoCaM bound to the IQ1 or IQ2 at a molar ratio of 1:1 increased by 4.8±0.3Å or 3.8±0.3Å, respectively, as compared with the corresponding crystal structure. The experimental Kratky plots indicated that apoCaM bound to the IQ1 or IQ2 adopts a dumbbell-shaped structure. In contrast to these complexes, the solution of apoCaM/IQ(1+2) at a molar ratio of 2:1 became turbid, indicating that the solution contains several types of aggregates. The turbid solution was centrifuged and the supernatant was used for the SAXS measurements. The SAXS results suggested that the supernatant is composed of a mixture of apoCaM/IQ(1+2) and apoCaM. The radius of gyration of apoCaM/IQ(1+2) at a molar ratio of 1:2 increased by 0.8±0.6Å, as compared with the corresponding crystal structure. The experimental Kratky plot was compared with calculated curves of both solution structures based on the dumbbell-shaped structure and the crystal structure.

Introduction

Myosins are a large family of molecular motors that move along actin filaments. Myosin II (conventional myosin) generates contraction in muscle, while myosin V (unconventional myosin) transports cargo as a monomer in non-muscle cells. All myosins have a globular N-terminal motor domain that contains the actin and ATP-binding sites, followed by an elongated α-helical lever arm (lever). The lever is composed of special sequences called IQ motifs (IQxxxRGxxxR, where consensus residues are underlined and x is any amino acid), each of which stabilized by the binding of calmodulin (CaM). Despite the prevalence of this motif in myosin, there was previously no atomic-resolution structure of a CaM-myosin heavy chain complex until recently.

Recently reported 2.5 Å resolution structure of calcium free CaM (apoCaM) bound to the first two IQ motifs of the murine myosin V heavy chain has revealed an unusual CaM conformation[1]. The C-terminal lobe of each CaM adopts a semi-open conformation that grips the first part of the IQ motif (IQxxxR), whereas the N-terminal lobe adopts a closed conformation that interacts more weakly with the second part of the motif (GxxxR). It is important to know whether the crystal structure is a stable structure even in solution, because a solution structure is directly

related to the function of myosin V.

In this report, we have investigated the solution structure of the complexes by small-angle X-ray scattering (SAXS) with use of synchrotron radiation as an intense and stable X-ray source, which is a useful method to detect direct interaction between CaM and target peptides through measurable structural changes of CaM. We used three synthetic peptides of residues 772-786 (IQ1), 795-810 (IQ2), and 772-810 (IQ(1+2)) of the myosin V to compare the solution structure with the crystal structure. The main SAXS results indicate that the solution structure is different from the corresponding crystal structure and that apoCaM bound to the IQ motif adopts a dumbbell-shaped structure.

Experimental

Materials. The recombinant CaM based on the sequence of rat CaM was expressed as described in ref. 2. CaM fraction was obtained as described in ref. 3. The peptides were synthesized and purified as described in ref. 4. Table 1 summarizes the primary sequences of three synthetic peptides, IQ1, IQ2, and IQ(1+2).

SR-SAXS Measurements. The basic medium used for the SAXS measurements was 50 mM Tris-HCl, pH 7.6, and 120mM NaCl. A complex of apoCaM with IQ1 or IQ2 was prepared by mixing 1.0 mol of the protein with 1.1 mol of the peptide and these solutions were clear. On the other hand, a complex of apoCaM with IQ(1+2) was prepared by mixing 1.0 mol of the protein with 0.5 mol of the peptide and the solution was turbid in the range of concentration from 3 to 10 mg/mL. The turbid solution was centrifuged and the supernatant was used for the measurements. Here the molar ratios of the peptide to the protein were determined according to ref. 1. The protein concentrations for both apoCaM/IQ1 and apoCaM/IQ2 were 7.5, 10.0, 12.5, 15.0, and 17.5 mg/mL, while those for apoCaM/IQ(1+2) were 2.26, 2.99, 5.6, and 8.7 mg/mL. The concentrations for both apoCaM/IQ1 and apoCaM/IQ2 were determined by the method described in ref. 5, while those for the supernatants of apoCaM/IQ(1+2) were determined spectroscopically.

Table 1: Primary Sequences of Three Peptides of IQ1, IQ2, and IQ(1+2) Synthesized in This Work

peptide name	primary sequence	AA[a]
IQ1	RIQKTIRGWLLRKRY	15
IQ2	TVQRYVRGYQARCYAK	16
IQ(1+2)	RIQKTIRGWLLRKRYLCMQRAAITVQRYVRGYQARCYAK	39

[a] AA represents the number of amino acid residues; Consensus residues are underlined; Abbreviations for the amino acid residues are: A, Ala; C, Cys; D, Asp; E, Glu; F, Phe; G, Gly; H, His; I, Ile; K, Lys; M, Met; N, Asn; P, Pro; Q, Gln; R, Arg; S, Ser; T, Thr; V, Val; W, Trp; and Y, Tyr.

The SAXS profiles for all samples were acquired using the instrument for SAXS installed at BL-10C of Photon Factory, KEK, Tsukuba. The details of the optics and instruments are given elsewhere[6]. An X-ray wavelength of 1.488 Å was used. The samples were contained in a mica cell with a volume of 70 μL, and the temperature was kept at 25.0±0.1℃ by circulating water through the cell holder. The reciprocal parameter, s, equals to $(2 \sin \theta)/\lambda$, was calibrated by the observation of a chicken collagen, where 2θ is the scattering angle and λ is the X-ray wavelength. Scattering data were collected for 300 s at various concentrations. Irradiation of all samples for periods up to 1800 s produced no change in the scattering profiles.

Scattering Data Analysis. Two methods of data analysis were used. The first method was that of Guinier and Fournet[7]. In the case of a group of identical particles, the scattering intensity of $I(s,c)$ measured as a function of s at a finite concentration, c, is given by

$$I(s,c) = I(0,c) \exp\{-(4\pi^2/3) R_g(c)^2 s^2\} \quad \text{(a)}$$

Here $I(0,c)$ is the scattering intensity at $s = 0$ and $R_g(c)$ is the radius of gyration at a concentration c. In the dilute limit, $I(0,c)$ and $R_g(c)$ are given by

$$Kc/I(0,c) = 1/M + 2A_2c + \cdots \quad \text{(b)}$$

$$R_g(c)^2 = R_0^2 - B_{if}c + \cdots, \quad \text{(c)}$$

respectively. Here K is an optical constant, M is the molecular weight of the protein, A_2 is the second virial coefficient, R_0 is the radius of gyration at infinite dilution, and B_{if} is the parameter of the interparticle interference[8]. The intercept and the initial slope of the Guinier plot (ln $I(s,c)$ versus s^2) determine $I(0,c)$ and $R_g(c)$, respectively. Using eqs. b and c, the four parameters M, A_2, R_0, and B_{if} are evaluated.

In the case of a group of several types of particles, an extended method of Guinier and Fournet was used[7]. In the dilute limit, $I(s,c)$ is given by

$$I(s,c) = \Sigma p_k I_k(s,c) \quad \text{(d)}$$

Here the summation encompasses all types of particles in the assemblage, p_k is the probability that one of the N particles is of the type k and $I_k(s,c)$ is the scattering intensity of the particle of type k. $I_k(s,c)$ is given by the same form as eq. a

$$I_k(s,c) = I_k(0,c) \exp\{-(4\pi^2/3) R_{gk}(c)^2 s^2\}, \quad \text{(a')}$$

By developing eq. a' under the condition of $(4\pi^2/3) R_{gk}(c)^2 s^2 << 1$ (the condition of Guinier), $I(s,c)$ is compiled into the same form as eq. a:

$$I(s,c) = I(0,c) \exp\{-(4\pi^2/3) R_{gz}(c)^2 s^2\} \quad \text{(e)}$$

But the intercept and the initial slope of the Guinier plot give the weight-average molecular weight (M_w) and the z-average radius of gyration (R_{gz}), respectively. M_w is obtained by

$$I(0,c) = \Sigma p_k I_k(0,c) = KcM_w, \quad \text{(f)}$$

where K is a optical constant and the total concentration c is given by:

$$c = \Sigma c_k \quad \text{(g)}$$

R_{gz} is given by

$$R_{gz}(c)^2 = \Sigma p_k I_k(0,c) R_{gk}(c)^2 / \Sigma p_k I_k(0,c) \quad \text{(h)}$$

The second method was that of Kratky, which is defined by the plot of $s^2 I(s)$ versus s (the Kratky plot) in the case of a group of identical particles[9]. The Kratky plots provide the structural characteristics (e.g., molecular shape) of a chain polymer and a biopolymer. The Kratky plot from a group of several types of particles was calculated by

$$s^2 I(s,c) / I(0,c) = s^2 \Sigma p_k I_k(s,c) / \Sigma p_k I_k(0,c) \quad \text{(i)}$$

Calculation of SAXS Profile of Known Tertiary Structures. PDB:2ix7 was used as the coordinates for the crystal structure. Coordinates for solution structures were newly created by separating the N-terminal lobe of apoCaM from the original position on the crystal structure. In the calculation of the scattering profiles, we fixed the radius of gyration of new solution structure to the value of 25.4 Å, whose value corresponds to that of apoCaM/IQ(1+2) at a molar ratio of 2:1. The scattering profiles were calculated by using the extended Debye's formula and normalized, as described previously[10].

Results

Guinier Region of the Scattering Profile. An example of Guinier plots for a complex of apoCaM/IQ1, apoCaM/IQ2, and apoCaM/IQ(1+2) over the concentration series is shown in Figure 1A-C. In all of the samples studied here, there is no evidence of any upward curvature at low s^2 values in the Guinier plots, which indicates that the data are free from the aggregation of samples. The values of $Kc/I(0,c)$ evaluated from the intercepts of the Guinier plots for all samples are shown in Figure 2A as a function of protein concentration. The plots are linear over the entire concentration range, and the value of $[Kc/I(0,c)]_{c=0}$ extrapolated to infinite dilution for each complex has the inverse molecular weight appropriate for the soluble particle. The slopes of these lines are positive for all complexes, indicating that the values of A_2 are positive, that is, the interaction between complexes is repulsive[8, 10, 11].

All values of molecular weight (M) in Table 2 agree well with the calculated values denoted in parentheses within the experimental error of about 7 %. Therefore, it is reasonable to conclude that apoCaM binds each peptide with the molar ratio described in Table 2.

Radii of gyration at infinite dilution (R_0) were

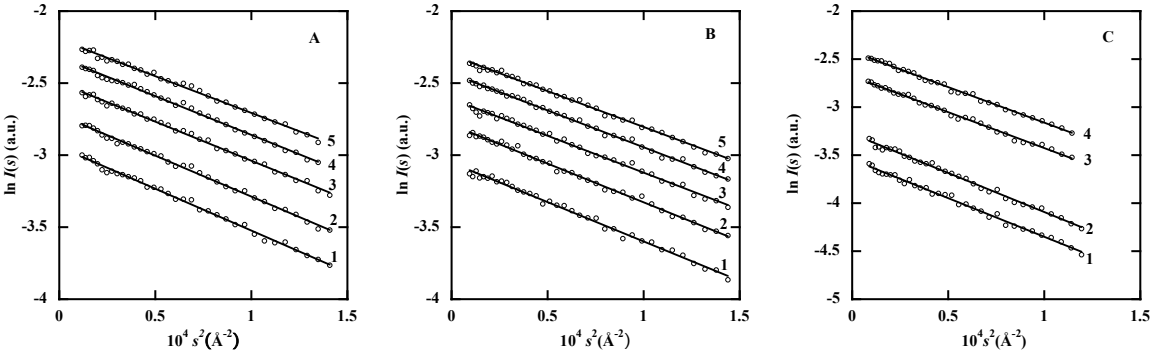

Figure 1: Guinier plots for a complex of apoCaM/IQ1 at a molar ratio of 1:1 (A), apoCaM/IQ2 at a molar ratio of 1:1 (B), and apoCaM/IQ(1+2) at a molar ratio of 2:1 (C) at various concentrations. The straight lines were obtained with the data points satisfying the Guinier condition by the least-squared method. (A) and (B): (1) 7.5 mg/mL; (2) 10.0 mg/mL; (3) 12.5 mg/mL; (4) 15.0 mg/mL; (5) 17.5 mg/mL. (C): (1) 2.26 mg/mL; (2) 2.99 mg/mL; (3) 5.6 mg/mL; (4) 8.7 mg/mL.

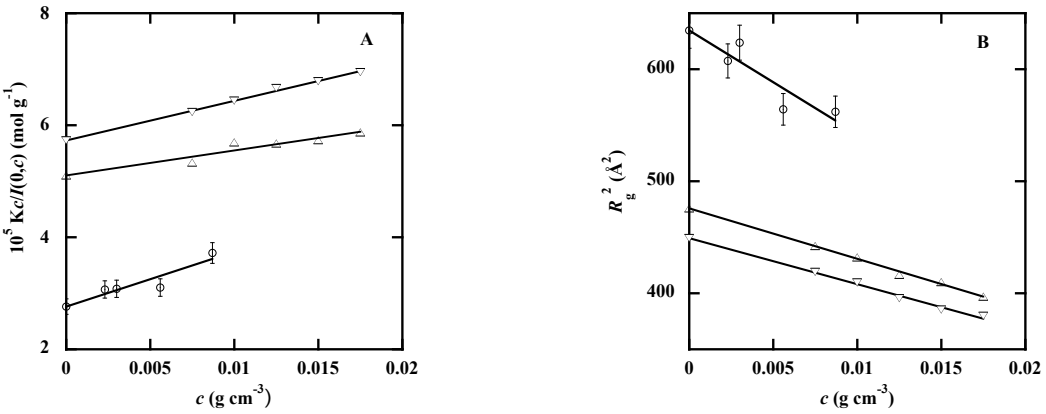

Figure 2: Zimm plots (A) and the square of the radius of gyration, R_g^2, (B) for a complex of apoCaM/IQ1, apoCaM/IQ2, and apoCaM/IQ(1+2). (△) apoCaM/IQ1 at a molar ratio of 1:1; (▽) apoCaM/IQ2 at a molar ratio of 1:1; (○) apoCaM/IQ(1+2) at a molar ratio of 2:1.

calculated from the slopes of the Guinier plots and are shown in Figure 2B. The linear increase with decreasing protein concentration was observed in all complexes. The slopes of these lines, which arise from interparticle interference effects, represent a virial coefficient[8, 10, 11]. Table 2 also compiles the values of R_0. The R_0 value for apoCaM/IQ1 and that for apoCaM/IQ2 are 21.8±0.3Å and 21.3±0.3Å, respectively, a value typical of the dumbbell-shaped structure[4, 11-13]. In contrast, the $R_{crystal}$ value for the crystal structure of apoCaM/IQ1 is 17.0Å and that for apoCaM/IQ2 is 17.5Å. The R_0 value of apoCaM bound to the IQ1 or IQ2 at a molar ratio of 1:1 increased by 4.8±0.3Å or 3.8±0.3Å, respectively, as compared with the corresponding structure, indicating that the solution structure is different from the crystal structure. In the crystal structure, the C-terminal lobe of each CaM adopts a semi-open conformation that grips the first part of the IQ motif (IQxxxR), while the N-terminal lobe adopts a closed conformation that interacts more weakly with the second part of the motif (GxxxR). The larger values of R_0 for apoCaM/IQ1 and apoCaM/IQ2 indicate that the N-terminal

Table 2: Molecular Weight (M), Radius of Gyration at Infinite Dilution (R_0) for a Complex of apoCaM/IQ1, apoCaM/IQ2, and apoCaM/IQ(1+2).

System	$10^{-3}M$ (g/mol) (calcd. value)[a]	R_0 (Å)	$R_{crystal}$ (Å)[b]
ApoCaM/IQ1 (1:1)	19.4±1.4 (18.7)	21.8±0.3	17.0
ApoCaM/IQ2 (1:1)	17.5±1.2 (18.7)	21.3±0.3	17.5
ApoCaM/IQ(1+2)(2:1)	35.9±2.5 (38.2)	25.2±0.6	24.6

[a] M for a complex of apoCaM/IQ1 and apoCaM/IQ2 at a molar ratio of 1:1, and apoCaM/IQ(1+2) at a molar ratio of 2:1.

[b] Radius of gyration for the corresponding crystal structure.

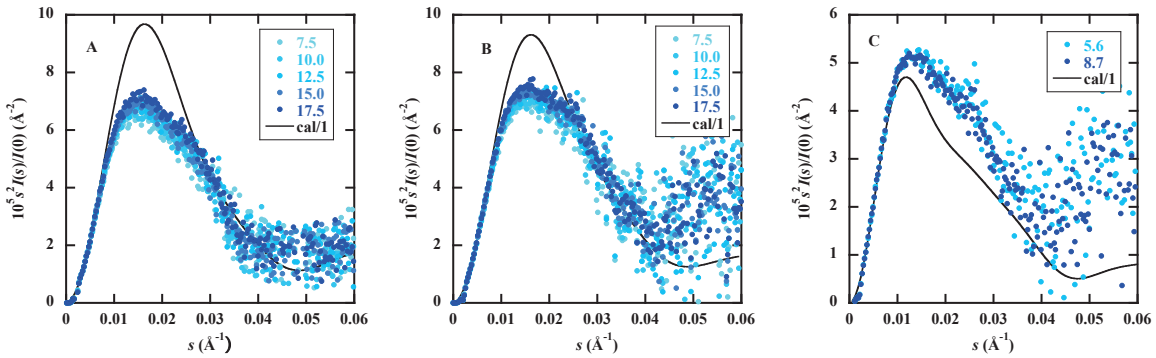

Figure 3: Kratky plots for a complex of of apoCaM/IQ1 at a molar ratio of 1:1 (A), apoCaM/IQ2 at a molar ratio of 1:1 (B), and apoCaM/IQ(1+2) at a molar ratio of 2:1(C) at various concentrations. The numbers in the frame of A-C denote concentrations of mg/mL. The black lines (cal/1) in A-C were calculated by using the corresponding atomic coordinates from the PDB: 2iX7.

lobe is separated from the second part of the motif in the solution. On the other hand, the R_0 value for apoCaM/IQ(1+2) is 25.2±0.6Å, whose value is slightly larger than the corresponding value of the crystal structure (24.6Å).

Kratky Region of the Scattering Profile. Figures 3A and 3B show the Kratky plots for apoCaM/IQ1 and apoCaM/IQ2, respectively, which are characterized by the presence of a broad peak near s = 0.015Å^{-1}, indicating that each complex adopts a dumbbell-shaped structure which is close to a dumbbell-shaped structure reported previously[4,10]. All scattering profiles converge to that at the highest concentration. On the other hand, the scattering profile calculated from the corresponding crystal structure is shown by a black solid line in Figures 3A or 3B, which is characterized by the presence of a sharp peak near s = 0.016Å^{-1}. From a comparison between these profiles, it is reasonable to conclude that the solution structure is obviously different from the corresponding crystal structure, suggesting that the N-terminal lobe of CaM is separated from the second part of IQ motif in the solution.

Figure 3C shows the Kratky plot for apoCaM/IQ(1+2), which is characterized by the presences of a broad and asymmetric peak near s = 0.013 Å^{-1} and a shoulder around s = 0.025Å^{-1}. In contrast, the calculated profile of the corresponding crystal structure (a black solid line), is characterized by the presences of a sharp peak near s = 0.011Å^{-1} and a shoulder around s = 0.025Å^{-1}. The results show that the profile calculated from only the crystal structure is not sufficient to reproduce the data points of the solution structure, suggesting that other components are contained.

Discussion

The measurements of the molecular weights, the radii of gyration and the Kratky plots for apoCaM/IQ1 and apoCaM/IQ2 presented here show that the solution structure adopts a dumbbell-shaped structure, whose structure is totally different from the crystal structure[1]. Combined with the results of the crystal structure, the most straightforward interpretation of the these SAXS results is that the N-terminal lobe of apoCaM is separated from the second part of the IQ motif in solution, while the C-terminal lobe still grips the first part of the motif.

In contrast, the scattering profiles calculated from the crystal structure for apoCaM/IQ(1+2) is not sufficient to reproduce the experimental profile, though the experimental values of M and R_0 are in good accordance with the calculated values for the crystal structure. In this point, we recall that an upward curvature

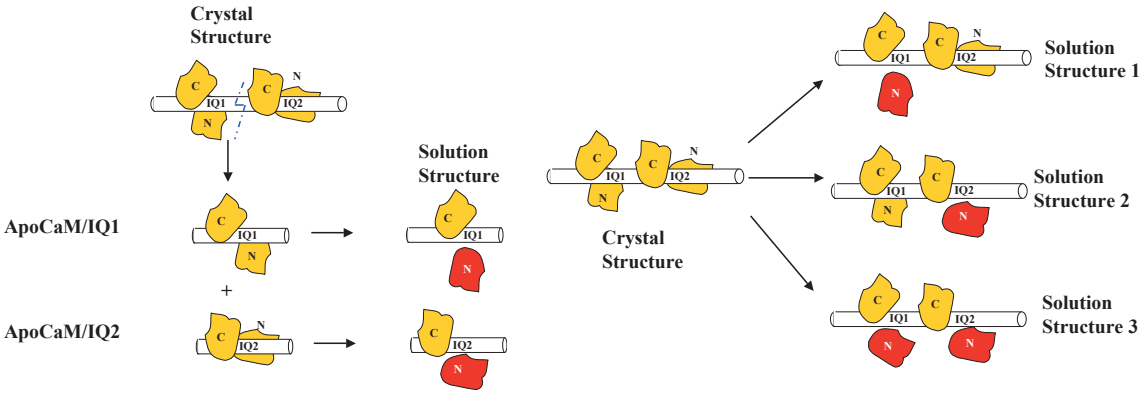

Figure 4: Crystal and solution structures for a complex of apoCaM/IQ1, apoCaM/IQ2, and apoCaM/IQ(1+2). In the crystal structure (PDB: 2ix7), the N-terminal lobe of apoCaM interacts with the second part (GxxxR) of IQ motifs, while the C-terminal lobe interacts with the first part (IQxxxR). In Figure 4A, the crystal structure was separated into two parts: apoCaM/IQ1 and apoCaM/IQ2. In Figure 4B, only the N-terminal lobe of apoCaM is separated from the second part of the IQ1 (the solution structure 1). In the solution structure 2, only the N-terminal lobe of apoCaM is separated from the second part of the IQ2. In the solution structure 3, each N-terminal lobe of apoCaM is separated from the second part of the corresponding IQ motif.

at low s^2 values in the Guinier plot was observed in a simple solution of IQ(1+2) (data is not shown), indicating that the solution contains various associates. A turbid solution was obtained by mixing the solution of IQ(1+2) with that of apoCaM. After the centrifugation, the supernatant was separated from the precipitates and used for the SAXS measurements. From the experimental values of M and R_0, it is clear that the main component of the supernatant is composed of the complex of apoCaM/IQ(1+2) at a molar ratio of 2:1. Noting that the value of M is smaller than the calculated value, other components with a lower molecular weight might be contained. Here, we assume that apoCaM is contained in the supernatant as a minor component. Then, the radius of gyration and molecular weight for apoCaM/IQ(1+2) are replaced by M_w in eq. f and R_{gz} in eq. h, respectively. Using M_w defined by $\Sigma\, p_k M_k^2 / \Sigma\, p_k M_k$, the experimental value of M_w (35.9×10^3) was reproduced by selecting $p_1 = 0.8$ for apoCaM/IQ(1+2) and $p_2 = 0.2$ for apoCaM, respectively. Using these values of p_1 and p_2, the value for the radius of gyration of apoCaM/IQ(1+2) at a molar ratio of 2:1 was evaluated as 25.4 Å. The results indicate that the component of apoCaM should be subtracted in advance from the experimental data in Figure 3C.

Furthermore, the results of apoCaM/IQ1 and apoCaM/IQ2 showed that the solution structure is evidently different from the corresponding crystal structure. Figure 4A shows a schematic solution structure for apoCaM/IQ1 or apoCaM/IQ2, in which the N-terminal lobe of apoCaM is separated from the second part of the IQ motif. Two types of solution structures are shown. Figure 4B shows three types of solution structures for apoCaM/IQ(1+2).

Figure 5 shows the calculated results of the scattering profiles for three types of solution structures as well as the crystal structure in Figure 4B. The data points for apoCaM/IQ(1+2) at a molar ratio of 1:2 are reproduced by these calculated profiles. By using the solution structures, a difference observed near s = 0.01 Å^{-1} is fairly improved. However, a difference in the range of 0.01< s (Å^{-1}) <0.03 is not substantially improved by the use of the solution structure. A further search of coordinates for an appropriate solution structure will be desired to improve this point. Research is in progress along this line.

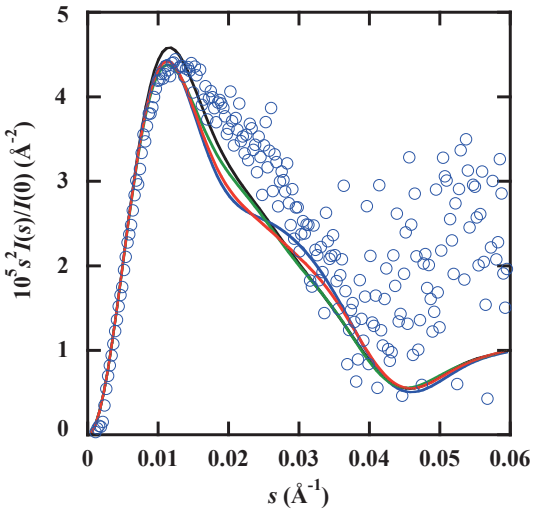

Figure 5: Comparison among the scattering curves corresponding to three types of structures shown in Figure 4B. The data points (open blue circles) were obtained by subtracting the data points for apoCaM from those for apoCaM/IQ(1+2), taking into account of the percentage. The black solid line denotes the crystal structure; the blue solid line denotes the solution structure 1; the green solid line denotes the solution structure 2; the red solid line denotes the solution structure 3.

Acknowledgments

We thank Dr. Katsumi Kobayashi for his help in the SAXS measurements at KEK and Dr. Nobuhiro Hayashi of Tokyo Institute of Technology for providing plasmids for the expression of CaM in *Escherichi coli* and for the spectroscopic determination of protein concentrations. The SAXS measurements were performed with approval of the Photon Factory Committee, KEK, Tsukuba, Japan (Proposal Nos. 05G299, 07G545 and 09G068).

References

1) A. Houdusse, J.-F. Gaucher, E. Krementsova, S. Mui, K.M. Trybus, and C. Cohen: Crystal structure of apo-calmodulin bound to the first two IQ motifs of myosin V reveals essential recognition features, PNAS 103-51, pp.19326-19331(2006).

2) N. Hayashi, M. Matsubara, A. Takasaki, K. Chitani, and H. Taniguchi: An expression system of rat calmodulin using T7 phage promoter in Escherichia coli, Protein Expression Purif. 12-1, pp. 25-28 (1998).

3) M. Yazawa, M. Sakuma, and K. Yagi: Calmodulins from muscles of marine invertebrates, scallop and sea anemone, J. Biochem. (Tokyo) 87-5, pp.1313-1320 (1980).

4) Y. Izumi, S. Kuwamoto, Y. Jinbo, and H. Yoshino: Increase in the molecular weight and radius of gyration of apocalmodulin induced by binding of target peptide: Evidence for complex formation, FEBS Lett. 495-1&2, pp.126-130 (2001).

5) O. H. Lowery, N .J. Rosenbrough, A. L. Farr, and R. J. Randall: Protein measurement with the Folin phenol reagent, J. Biol. Chem. 193-1, pp. 265-275 (1951).

6) T. Ueki, Y. Hiragi, M. Kataoka, Y. Inoko, Y. Amemiya, Y. Izumi, H. Tagawa, and Y. Muroga: Aggregation of bovine serum albumin upon cleavage of its disulfide bonds, studied by the time-resolved small-angle X-ray scattering technique with synchrotron radiation, Biophys. Chem. 23-1&2, pp.115-124 (1985).

7) A. Guinier and G. Fournet, Small-Angle Scattering of X-Rays, John Wiley & Sons, New York (1955) pp. 65-67 & pp.126-129.

8) Y. Izumi, M. Wakita, H. Yoshino, and N. Matsushima: Structure of the proteolytic fragment F34 of calmodulin in the absence and presence of mastoparan as revealed by solution scattering, Biochemistry 31-48, pp.12266-12271 (1992).

9) O. Kratky, in Small-Angle X-ray Scattering (Edited by H. Brumberger), Gordon & Breach, Science Publishers, New York (1967) pp.63-129.

10) Y. Izumi, H. Watanabe, N. Watanabe, A. Aoyama, Y. Jinbo, and N. Hayashi: Solution X-ray scattering reveals a novel structure of calmodulin complexed with a binding domain peptide from the HIV-1 matrix protein p17, Biochemistry 47-27, pp. 7158-

7166 (2008).
11) T. Yokouchi, H. Nogami, Y. Izumi, H. Yoshino, K. Nakashima, and M. Yazawa: Solution X-ray scattering data show structural differences among chimeras of yeast and chicken calmodulin: Implications for structure/function, Biochemistry 42-7, pp. 2195-2201(2003).
12) N. Matsushima, Y. Izumi, T. Matsuo, H. Yoshino, T. Ueki, and Y. Miyake: Binding of calcium and mastoparan to calmodulin induces a large change in the tertiary structure, J. Biochem. (Tokyo) 105-6, pp. 883-887 (1989).
13) M. Noguchi, Y. Izumi, and H. Yoshino: Target recognition by calmodulin: the role of acid region contiguous to the calmodulin-binding domain of calcineurin A, FEBS Lett. 573-1~3, pp.121-126 (2004).